Theor Chem Acc (2000) 103:518–523
DOI 10.1007/s002149900085

Theoretical
Chemistry Accounts

Regular article

Transport properties of boron and aluminum

Eugene Levin[1], **James R. Stallcop**[2], **Harry Partridge**[2]

[1] Thermosciences Institute, M/S 230-3, NASA Ames Research Center, Moffett Field, CA 94035-1000, USA
[2] Computational Chemistry Branch, M/S 230-3, NASA Ames Research Center, Moffett Field, CA 94035-1000, USA

Received: 9 July 1999 / Accepted: 18 August 1999 / Published online: 2 November 1999
© Springer-Verlag 2000

Abstract. Transport cross sections and collision integrals are tabulated for a wide range of energies and temperatures for the interactions B–B and Al–Al. For aluminum, a semiclassical approximation was used to determine the scattering phase shifts from which the transport cross sections were calculated. For boron, the smaller reduced mass and the deep potential wells required the phase shifts at lower energies to be determined from a numerical solution of the time-independent Schroedinger equation; the semiclassical approximation was used at higher energies where the two methods agree. The variations of the collision integrals for viscosity and diffusion are presented graphically as a function of temperature. The results are applied to estimate the transport properties of gallium.

Key words: Transport properties – Cross sections – Collision integrals – Scaling relations – Scattering

1 Introduction

The transport properties of atom–atom interactions are needed for studies of gases and plasmas such as those of the high-temperature environment for aeroentry into planetary atmospheres, processes for the construction or preparation of certain electronic devices [1], and for the study of stellar atmospheres. With the exception of interactions involving rare-gas atoms, these properties cannot be measured in the laboratory by the usual methods because of the difficulty in producing gases with a pure species concentration. Simplified approximations for the determination of atom–atom transport data are often based on inappropriate potential functions with parameters that are constructed from questionable empirical rules. On the other hand, the accurate theoretical determination of transport properties, in general, is a laborious procedure since it requires a complete set of interaction energies corresponding to all possible paths available to the collision.

For interactions in which one of the collision partners is a rare-gas atom such as helium, the computational effort required for an accurate theoretical determination is comparatively simple and studies are underway to develope Aufbau relations from which the transport properties of an X–X interaction can be inferred from the properties of He–He and He–X interactions. The verification of the accuracy of these models requires that the transport properties of test cases of the difficult X–X interactions be known for comparison with predictions based on combining rules using He–X results.

The availability of complete sets of potential-energy curves [2, 3] for B–B and Al–Al interactions permits the calculation of the transport cross sections and the collision integrals for these interactions. Moreover, since the boron and aluminum atoms have the same spin and angular quantum numbers, the scattering results provide a test of candidate procedures for predicting transport cross sections from the interactions of these atoms with helium.

The computational methods are outlined in Sect. 2 and the salient properties of the interaction potentials for boron and aluminum are described in Sect. 3. The resulting transport cross sections and collision integrals as a function of temperature for B–B and Al–Al are presented in Sect. 4 and are used to estimate the transport properties of gallium. Section 5 contains concluding remarks.

2 Method

According to Chapman – Enskog theory [4–6], the transport properties of dilute monatomic gases can be expressed in terms of the mean collision integrals,

$$\bar{\Omega}_{n,s}(T) = \frac{F(n,s)}{2(k_B T)^{s+2}} \int_0^\infty \exp^{(-E/k_B T)} E^{s+1} \bar{Q}_n(E) \mathrm{d}E \ , \qquad (1)$$

where $\bar{Q}_n(E)$ is the mean transport cross section [$\bar{Q}_1(E)$ is related to momentum transfer and $\bar{Q}_2(E)$ is related to energy transfer], k_B is the Boltzmann constant, T is the kinetic temperature, and $F(n,s)$ is obtained from the relation

Correspondence to: E. Levin

$$F(n,s) = \frac{4(n+1)}{\pi(s+1)![2n+1-(-1)^n]} \quad . \tag{2}$$

The transport cross sections, $Q_n(E)$, can be obtained from the scattering phase shifts, η_l, which are calculated from the adiabatic interaction energy of a given state of the molecule formed from the colliding particles, i.e.,

$$Q_n(E) = \frac{4\pi}{k^2} \sum_{l=0}^{\infty} \sum_{v>0}^{n} a_{nv}^{l} \sin^2(\eta_{l+v} - \eta_l) \quad , \tag{3}$$

where l is the angular momentum quantum number, k is the wave number, and the allowed values of v are even or odd according to the parity of n. The coefficients a_{nv}^{l} can be determined by recursion from

$$(2l+1)x^n P_l(x) = \sum_{v=-n}^{n} a_{nv}^{l} P_{l+v}(x) \quad , \tag{4}$$

where $P_l(x)$ is a Legendre polynomial. When the colliding pair can interact through more than one state, the mean transport cross section, $\bar{Q}_n(E)$, the degeneracy-weighted average of the cross sections for all states, is the quantity used for the determination of transport properties at high temperatures [6].

The above formulation is independent of the method used to determine η_l. The difference between the semiclassical and quantum mechanical approaches lies in the method for calculating these phase-shifts. The semiclassical method is based on a uniform phase-shift approximation due to Stallcop [7]. This approximation accounts for tunneling through the barrier of the effective potential energy and also accounts for resonance scattering associated with metastable energy levels of the inner potential well and virtual energy levels above the barrier maximum. The detailed formulation of the semiclassical phase-shift approximation can be found in our previous work [8, 9].

For strongly bound interactions of small reduced mass, the phase shifts must be determined quantum mechanically at the lower kinetic energies. The method used to compute the phase shifts quantum mechanically combines the techniques of **R**-matrix propagation [10] and Richardson extrapolation [11]. This method is computationally efficient and has been presented in detail in Ref. [12].

3 Interaction Potentials

Accurate ab initio potential-energy curves for the atomic interactions of B–B and Al–Al were determined by Langhoff and Bauschlicher [2, 3], and the ground-state singlet and triplet potentials are shown in Figs. 1 and 2. More recent benchmark calculations [13–15] have confirmed the high quality of these interaction potentials. From Eq. (1) it follows that the determination of collision integrals over a wide range of temperatures requires the calculation of transport cross sections for a wide range of energies. The calculations were performed using a code which accepts discrete potential-energy data from ab initio electronic structure calculations, incorporates the asymptotic form of the long-range potential, and, as necessary, extends the ab initio data at very short separation distances using an exponential extrapolation.

The ab initio results [2, 3] are extended at large values of the separation distance, r, using long - range expansions of the interaction energies. For very low energy applications, the spin-orbit interactions should be taken into account; however, for the temperatures of our present work, the ΛS coupling scheme of Refs. [2, 3] should be adequate. The effect of the spin-orbit interactions on transport data for low-temperature applications is discussed in Sect. 4. The leading electrostatic coefficient, C_5, of the term C_5/r^5 arises from the interaction of the quadrupole moments of the atoms. The values of these coefficients have been determined from the formulation of Chang [16] using the results of a relativistic Hartree–Dirac calculation [17]. The leading dispersion coefficients, C_6, have been obtained from the well-known combination rule [18]

$$\frac{\alpha(\mathrm{He})\alpha(X)}{C_6(\mathrm{He},X)} = \frac{1}{2}\left[\frac{\alpha(\mathrm{He})\alpha(\mathrm{He})}{C_6(\mathrm{He},\mathrm{He})} + \frac{\alpha(X)\alpha(X)}{C_6(X,X)}\right] \tag{5}$$

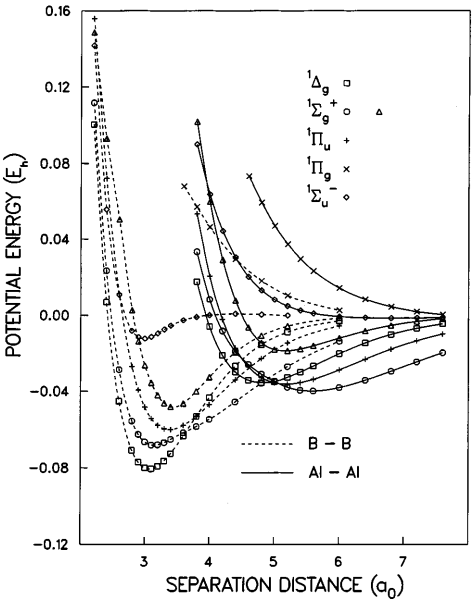

Fig. 1. Potential-energy curves for the singlet states of boron and aluminum

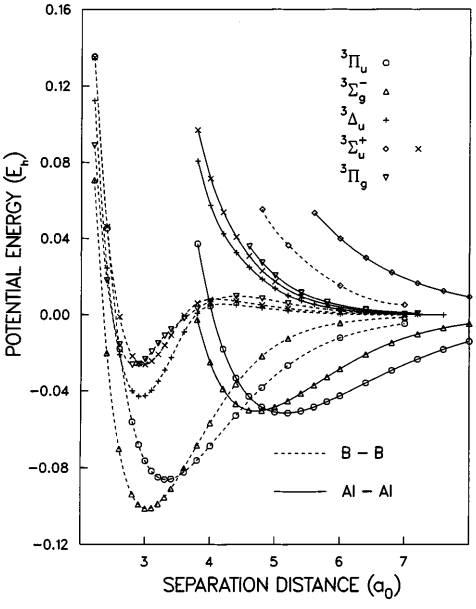

Fig. 2. Potential-energy curves for the triplet states of boron and aluminum

which is found [19] to be accurate to about 0.5%. The quantity α is the polarizability of the atom and X represents either boron or aluminum. The values of α are obtained from calculations [20–22] and the value of $C_6(\mathrm{He},\mathrm{He})$ is obtained from Ref. [20]. The values of $C_6(\mathrm{He},X)$ have been extracted from the results of a high-level calculation for interactions of atoms with helium. Specifically, a coupled-cluster singles and doubles approach [23] that includes a perturbational correction for triples [24] with large basis sets, atom-centered augmented correlation-consistent polarized-valence quadruple zeta of Dunning and coworkers [25–27] and midpoint-centered bond functions [28] is combined with a counterpoise method [29] to correct for basis-set superposition error and thereby obtain accurate energies. The small contribution to the interaction energy from higher-order dispersion terms needed to obtain accurate values of C_6 from the calculated results was approximated by the formulation of Starkshall and Gordon [30] using the calculated moments of Ref. [17].

The values of C_5 are listed in Table 1 and the values of C_6 are 77.03 for boron and 403.2 for aluminum. The values of $C_8(X,X)$ and $C_{10}(X,X)$ required for the present work were also obtained by the approximation previously described for the higher-order dispersion contributions. The interaction energies from the long-range expansion are joined to the calculated results of Refs. [2, 3] by exponential interpolation [8] or by a van der Waals potential function [31] when the exchange energy is attractive or repulsive, respectively.

From Figs. 1 and 2 it may be noted that each set of six curves for a certain molecular spin contains a pair of curves for $^1\Sigma_g^+$ states. From Table 1 it may be concluded that the molecule for the upper state dissociates into atoms that are repelled by the quadrupole–quadrupole interaction at large r, whereas the atoms of the lower state are attracted by the dispersion forces. The behavior of the potential curves for this pair of boron singlet states shown in Fig. 1 indicates that an avoided crossing occurs in the vicinity where the potential wells have a minimum. Note that the quadrupole–quadrupole interaction can account for the broad behavior of the potential-energy wells of certain states such as the lowest $^1\Sigma_g^+$, $^1\Pi_g$, and $^3\Pi_u$ states.

Table 1. Properties of singlet and triplet states for boron and aluminum: state degeneracy and C_5 coefficients of the long-range form of the potentials

State	Degeneracy	C_5 boron	C_5 aluminum
$^1\Delta_g$	2	9.1	47
$^1\Sigma_g^+$	1	0.0	0
$^1\Sigma_g^+$	1	54.8	284
$^1\Pi_u$	2	0.0	0
$^1\Pi_g$	2	−36.3	−188
$^1\Sigma_u^-$	1	0.0	0
$^3\Pi_u$	6	−36.3	−188
$^3\Sigma_g^-$	3	0.0	0
$^3\Delta_u$	6	9.1	47
$^3\Sigma_u^+$	3	0.0	0
$^3\Sigma_u^+$	3	54.8	284
$^3\Pi_g$	6	0.0	0

At separation distances shorter than those of the ab initio calculations, as shown in Figs. 1 and 2, the data were extended using an exponential fit to obtain cross-section data at high energies. From Eq. (1) it can be shown that for temperatures of 3000 K collision cross sections at energies up to about 0.15 E_h are needed for an accurate approximation to the integral. It should be noted that this extrapolation using an assumed form for the short-range potential slightly degrades the overall accuracy of the final results for the collision integrals at high temperatures.

4 Transport cross sections and collision integrals

The collision integrals are relatively insensitive to small variations in the reduced mass, especially at higher temperatures where the scattering can be described well by classical mechanics; hence, we have used standard atomic weights [32] for the present calculations. For aluminum interactions, using a reduced mass of 13.4908 amu, the potential wells shown in Figs. 1 and 2 are relatively shallow and it was found that the semiclassical method was adequate. For boron interactions the potential wells are deeper; using a reduced mass of 5.4055 amu, it was necessary to determine the phase shifts quantum mechanically at the lower energies. The semiclassical method was then used above the energies for which the two methods differed by less than 3 units in the fourth significant figure.

The mean cross sections needed to determine the collision integrals are obtained by combining the 12 states weighted according to their degeneracy as shown in Table 1. The resulting mean transport cross sections, $\bar{Q}_1$, $\bar{Q}_2$, and $\bar{Q}_3$, are shown in Table 2 for a range of interaction energies. Once the $\bar{Q}_i$ are known, Eq. (1) may be used to calculate the mean collision integrals, $\bar{\Omega}_{n,s}$, as a function of temperature. The four collision integrals shown in Table 3 are sufficient to calculate transport properties of binary gas mixtures to first order [4]. Additional collision integrals sufficient for higher-order calculations of multiple gas mixtures can be obtained using the $\bar{Q}_n$ of Table 2 in Eq. (1) or upon request from the authors.

The truncated ranges of Tables 2 and 3 for aluminum reflect the effects of spin-orbit coupling as discussed below.

For pure gases, the transport coefficients for diffusion, viscosity and thermal conductivity respectively, $D(T)$, $\eta(T)$ and $\lambda(T)$ are defined in terms of the collision integrals, $\bar{\Omega}$, by

$$10^4 T^{-3/2} p D(T) = 26.287(2\mu)^{-1/2}/\bar{\Omega}_{1,1}(T) \ , \tag{7}$$

$$10^6 T^{-1/2} \eta(T) \quad = 26.696(2\mu)^{1/2}/\bar{\Omega}_{2,2}(T) \ , \tag{8}$$

$$10^5 T^{-1/2} \lambda(T) \quad = 19.891(2\mu)^{-1/2}/\bar{\Omega}_{2,2}(T) \ , \tag{9}$$

where D is in centimeters squared per second, η is in grams per centimeter second, λ is in calories per centimeter second, T is in Kelvin, pressure, p, is in atmospheres, reduced mass, $\mu = M_1 M_2/(M_1 + M_2)$, is in

Table 2. Mean transport cross sections, $\bar{Q}_i$ (a_0^2), for boron and aluminum

E(E_h)	Boron			Aluminum		
	$\bar{Q}_1$	$\bar{Q}_2$	$\bar{Q}_3$	$\bar{Q}_1$	$\bar{Q}_2$	$\bar{Q}_3$
0.00010	574.96	494.05	688.83			
0.00015	466.80	395.35	577.49			
0.00020	404.56	341.98	500.24			
0.00030	335.15	288.60	414.41			
0.00050	269.69	225.69	330.82	518.35	431.70	625.37
0.00070	236.94	199.36	288.23	451.75	372.87	546.02
0.00100	205.83	174.47	247.66	399.68	323.03	476.61
0.00150	197.39	157.38	232.87	340.61	282.31	407.00
0.00200	165.64	136.52	196.83	304.46	254.10	366.35
0.00300	149.04	120.05	174.50	265.19	216.98	316.61
0.00500	136.44	106.17	157.07	223.71	181.56	265.04
0.00700	121.43	96.52	141.06	204.36	162.00	239.37
0.01000	118.87	92.31	137.95	187.71	146.20	217.57
0.01500	107.23	82.67	126.18	169.86	130.61	195.71
0.02000	91.19	70.89	108.31	158.00	122.07	182.07
0.03000	83.72	63.59	97.62	141.19	110.62	163.38
0.05000	65.27	51.41	76.60	103.40	100.53	129.74
0.07000	54.00	48.95	65.59	80.56	84.09	110.51
0.10000	40.69	42.49	54.88	64.08	66.03	89.55
0.15000	29.32	31.96	42.69	51.54	51.21	70.09
0.20000	24.01	25.52	34.76	44.96	43.83	59.88
0.30000	18.92	19.24	26.36	37.59	36.17	49.16

Table 3. Mean collision integrals $\bar{\Omega}_{1,1}$, $\bar{\Omega}_{1,2}$, $\bar{\Omega}_{1,3}$, and $\bar{\Omega}_{2,2}$ (Å^2) for boron and aluminum

T(K)	Boron				Aluminum			
	$\bar{\Omega}_{1,1}$	$\bar{\Omega}_{1,2}$	$\bar{\Omega}_{1,3}$	$\bar{\Omega}_{2,2}$	$\bar{\Omega}_{1,1}$	$\bar{\Omega}_{1,2}$	$\bar{\Omega}_{1,3}$	$\bar{\Omega}_{2,2}$
100	21.25	18.60	17.07	23.22				
200	16.72	14.94	13.83	18.25				
300	14.77	13.34	12.46	16.08	26.48	23.34	21.38	28.65
400	13.62	12.43	11.76	14.86	23.94	21.22	19.58	25.83
500	12.90	11.89	11.36	14.11	22.23	19.87	18.58	23.98
600	12.37	11.46	10.85	13.53	21.01	18.88	17.62	22.63
700	11.95	11.07	10.44	13.02	20.06	18.11	16.86	21.56
800	11.62	10.85	9.90	12.58	19.35	17.45	16.15	20.68
900	11.36	10.42	9.67	12.19	18.66	16.92	15.83	19.97
1000	11.01	10.13	9.44	11.83	18.12	16.47	15.42	19.38
1200	10.52	9.56	8.90	11.17	17.25	15.72	14.69	18.43
1400	10.10	9.17	8.45	10.67	16.56	15.08	14.04	17.70
1600	9.66	8.79	8.06	10.21	15.97	14.52	13.41	17.10
2000	9.08	8.14	7.42	9.45	15.00	13.53	12.37	16.16
2400	8.57	7.61	6.89	8.87	14.18	12.66	11.42	15.44
3000	7.94	6.97	6.29	8.23	13.14	11.51	10.27	14.55

atomic mass units, and the collision integrals, $\bar{\Omega}$, are in angstroms squared.

The principal collision integrals $\bar{\Omega}_{1,1}$ and $\bar{\Omega}_{2,2}$ are shown in Fig. 3. As noted in Sect. 3, the ab initio potentials were extended at small separation distances by an exponential extrapolation. Consequently the accuracy of the mean cross sections at high energies (and hence the collision integrals at high temperatures) is degraded by this assumed form of the potentials. The severity of the degradation depends on the extent to which the true potentials at short range differ from an exponential form. The curves shown in Fig. 3 up to approximately

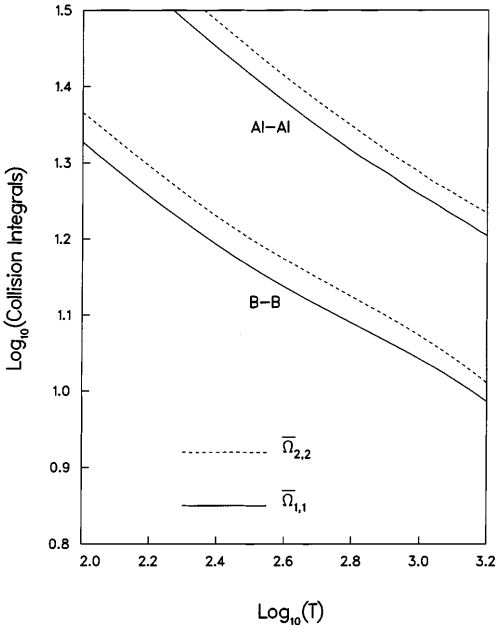

Fig. 3. Mean collision integrals $\bar{\Omega}_{1,1}$ and $\bar{\Omega}_{2,2}$ as functions of temperature

1500 K are substantially free of this possible degradation and are based on the ab initio potentials and the long-range form of the potential. Above this temperature, there is an increasing contribution from the extrapolated potentials, reaching approximately 6% due to such extrapolations at 3000 K.

At very low temperatures the effects of spin-orbit interaction must be considered. At large r, the molecular states are described by wave functions $|S\Lambda\Omega>$ that include spin-orbit coupling rather than $|S\Lambda>$ for the coupling scheme applied above. The $|S\Lambda\Omega>$ potential-energy curves could be determined from ab initio calculations with bond functions and a perturbation approximation to include the spin-orbit interaction. To avoid the large computational effort required for this direct approach, we take a more expedient way to assess the spin-orbit effects.

We modify the scattering treatment to take the fine structure of the atom into account. The potential energies of the $|S\Lambda\Omega>$ are represented by the $|S\Lambda>$ potential energies that are described above, but are shifted in energy by an amount NE_s, where the splitting energy E_s is taken from Ref. [33] and N is an integer (0–2) that is based on the correlations between the two coupling schemes and is consistent with the energy ordering found in Refs. [2, 3]. The degeneracy factor is either 1 or 2 depending upon whether the quantum number Ω is 0 or greater than 0, respectively. The occupations of the asymptotic ($r \rightarrow \infty$) excited states are represented by Boltzmann factors for thermodynamic equilibrium.

We find that the results can be specified by a shift, ΔT, such that the collision integral $\Omega_{n,n}(T)$ that accounts for the atomic fine structure is nearly the same as $\bar{\Omega}_{n,n}(T - \Delta T)$ of Table 3. The values of ΔT for $\Omega_{2,2}(T)$ and $\Omega_{1,1}(T)$, are only about 6 and 7 K, respectively, for boron, whereas, the respective values rise to about 60

and 70 K for aluminum. The difference between $\Omega_{2,2}(T)$ and $\bar{\Omega}_{2,2}(T)$ is only about 1% at 200 K for boron, but is larger by about 6% at 300 K for aluminum.

ΔT provides a temperature gauge to estimate the lowest T such that the spin-orbit interaction can be neglected for transport calculations. Improved low-T transport data might be most readily obtained following the method of Cohen and Schneider [34], which allows the $|S\Lambda\Omega>$ potential energies to be constructed from the $|S\Lambda>$ potential energies using a spin-orbit interaction that is determined from measured data for the atom. A detailed study to determine accurate low-T transport data is, however, outside the scope of our present investigation.

Note that the collision integrals of Fig. 3 exhibit a strong correlation, i.e., the collision integrals for aluminum have approximately the same slope with respect to temperature as the corresponding integrals for boron, but are shifted to a larger value. This is not surprising in that the behavior of the potential curves for boron interactions shown in Figs. 1 and 2 are found to be correlated to the behavior of the potential curves of aluminum with the same symmetry, but with repulsive walls that are shifted to a larger value of r. For example, a strongly bound boron state corresponds to a bound aluminum state of the same symmetry (but with a well that is broadened and shallower). Similarly, a weakly bound boron state is related to a weakly bound (or repulsive) aluminum state and a repulsive boron state corresponds to a repulsive aluminum state.

It may also be observed from Fig. 3 (and Table 3) that the collision integrals can be approximated by a log-linear relationship at higher T, for example,

$$\log(\bar{\Omega}_{2,2})_{\mathrm{Al}} \approx 2.174 - 0.294 \log(T) \qquad (10)$$

for T above 300 K.

The similarity in slope of the collision integrals is also found [8] for other members of the first row of the periodic chart that have electrons in the p valence shell. This leads one to expect that the scaling parameter [35] that specifies the size of the atom is the dominant factor for estimating the magnitude of transport collision integrals for collisions among P-state atoms. This contrasts with the scaling found [35] for collisions where the effective potential for the scattering can be described by a van der Waals interaction; in those cases, the scaling parameter [4], ϵ, has a simple physical interpretation such as the well depth [36] of the orientation-averaged interaction energy.

As an application of these observations, note that gallium occupies the same column in the periodic chart as boron and aluminum (all have a common ground state, $^2P_{1/2}$) and, consequently, the present results may be used to obtain an estimate of the transport properties of gallium. At high temperatures the collision integrals vary [35] as the square of a characteristic length scaling factor σ. For correlation of measured data Bzowski et al. [35] have shown that a satisfactory value for σ is the separation distance for which the effective interaction energy vanishes. Effective X–X interaction energies can be readily obtained from calculated He–X results by adapting the method of Ref. [31] to provide estimates of the ratio of characteristic lengths: using the quadruple zeta basis set of Bauschlicher [36] for gallium, this approach yields a gallium–aluminum ratio of 0.9285. From Eq. (10) and the scaling relation $(\bar{\Omega}_{2,2})_{\mathrm{Ga}}/(\bar{\Omega}_{2,2})_{\mathrm{Al}} = \sigma^2_{\mathrm{Ga}}/\sigma^2_{\mathrm{Al}}$ we estimate that the viscosity collision integral for gallium is given by

$$\log(\bar{\Omega}_{2,2})_{\mathrm{Ga}} \approx 2.11 - 0.294 \log(T) \qquad (11)$$

and that the viscosity–diffusion ratio [4], A^*, is approximately 1.07 for boron, aluminum, and gallium interactions in the range 300 K $< T <$ 3000 K. Note, however, that these results do not include spin-orbit effects for gallium.

5 Conclusions

Mean transport cross sections and collision integrals have been tabulated for B–B and Al–Al interactions. The slopes of $\log(\bar{\Omega})$ plotted with respect to $\log T$ are found to be nearly constant for temperatures above 300 K as in other atom–atom interactions [8]. Furthermore the slopes for boron and aluminum are approximately the same. The values of $\bar{\Omega}_{1,1}$ and $\bar{\Omega}_{2,2}$ for Al–Al are found to be larger than the corresponding values for B–B; this is expected since the interaction potentials of the corresponding states are highly correlated but are shifted to a larger value of the atom–atom separation distance, thus resulting in larger collision cross sections. A scaling application of the present results is illustrated by estimating the transport properties of gallium.

Acknowledgements. The authors thank S.R. Langhoff and C.W. Bauschlicher for providing their ab initio results and asymptotic values of the energies. We also wish to thank the referee for helpful suggestions regarding long-range spin-orbit effects. The work of E.L. was supported by contract NAS2-14031 from NASA to the Eloret Corporation.

References

1. Meyyappan M (ed) (1995) Computational modeling in semiconductor processing. Artech House, Boston
2. Langhoff SR, Bauschlicher CW (1990) J Chem Phys 92: 1879
3. Langhoff SR, Bauschlicher CW (1991) J Chem Phys 95: 5882
4. Maitland GC, Rigby M, Smith EB, Wakeham WA (1981) Intermolecular forces, their origin and determination. Oxford University Press, Oxford
5. Chapman S, Cowling TG (1970) The mathematical theory of non-uniform gases, 3rd edn. Cambridge University Press, New York
6. Hirshfelder JO, Curtiss CF, Bird RB (1964) Molecular theory of gases and liquids. Wiley-Interscience, New York
7. Stallcop JR (1969) Semiclassical elastic scattering cross sections for a central field potential function. Scientific and Technical Information Division, NASA SP-3052
8. Levin E, Partridge H, Stallcop JR (1990) J Thermophys Heat Transfer 4: 469
9. Stallcop JR, Partridge H, Levin E (1991) J Chem Phys 95: 6429
10. Truhlar DG, Harvey NM, Onda K, Brandt MA (1979) In: Thomas L (ed) Algorithms and computer codes for atomic and molecular scattering theory. National Resource for Computation in Chemistry, Berkeley, Calif., p 220
11. Press WH, Flannery BP, Teukolsky SA, Vetterling WT (1986) Numerical recipes. Cambridge University Press, Cambridge

12. Levin E, Schwenke DW, Stallcop JR, Partridge H (1994) Chem Phys Lett 227: 669
13. Peterson KA, Kendall RA, Dunning TH (1993) J Chem Phys 99: 9790
14. Woon DE, Dunning TH (1994) J Chem Phys 101: 8877
15. Peterson KA, Wilson AK, Woon DE, Dunning TH (1997) Theor Chem Acc 97: 251
16. Chang TY (1967) Rev Mod Phys 39: 911
17. Desclaux JP (1973) At Data Nucl Data Tables 12: 311
18. Kramer HL, Hershbach DR (1970) J Chem Phys 53: 2792
19. Thakkar AJ (1984) J Chem Phys 81: 1919
20. Bishop DM, Pipin J (1993) Int J Quantum Chem 45: 349
21. Werner H, Meyer W (1976) Phys Rev A 13: 13
22. Reinsch E, Meyer W (1976) Phys Rev A 14: 915
23. Bartlett RJ (1981) Annu Rev Phys Chem 32: 359
24. Raghavachari K, Trucks GW, Pople JA, Head-Gordon M (1989) Chem Phys Lett 157: 479
25. Dunning TH (1989) J Chem Phys 90: 1007
26. Kendall RA, Dunning TH, Harrison RJ (1992) J Chem Phys 96: 6796
27. Woon DE, Peterson KA, Dunning TH (1993) J Chem Phys 98: 1358
28. Tao F-M, Pan Y-K (1992) J Chem Phys 97: 4989
29. Boys SF, Bernardi F (1970) Mol Phys 19: 533
30. Starkshall G, Gordon RG (1972) J Chem Phys 56: 2801
31. Stallcop JR, Bauschlicher CW, Partridge H, Langhoff SR, Levin E (1992) J Chem Phys 97: 5578
32. IUPAC Commission on Atomic Weights and Isotopic Abundances (1995) J Phys Chem Ref Data 24: 1561
33. Moore CE (1971) Atom energy levels. National Bureau of Standards, Washington, D.C.
34. Cohen JS, Schnieder B (1974) J Chem Phys 61: 3230
35. Bzowski J, Kestin J, Mason EA, Uribe FJ (1990) J Phys Ref Data 19: 1179
36. Bauschlicher CW (1998) J Phys Chem A 102: 10424